Talanta 214 (2020) 120842

Contents lists available at ScienceDirect

Talanta

journal homepage: www.elsevier.com/locate/talanta

Execution of aggregation-induced emission as nano-sensors for hypochlorite detection and application for bioimaging in living cells and zebrafish

Hong Chen[a,b,1], Xiaojun He[c,1], Yuzhong Yu[a], Yuna Qian[d], Jianliang Shen[c,d,*], Shanchao Zhao[a,**]

[a] Department of Urology, Nanfang Hospital, Southern Medical University, Guangzhou, 510515, China
[b] Luoyang Key Laboratory of Organic Functional Molecules, College of Food and Drug, Luoyang Normal University, Luoyang, 471934, China
[c] School of Ophthalmology & Optometry, School of Biomedical Engineering, Wenzhou Medical University, Wenzhou, 325035, China
[d] Wenzhou Institute, University of Chinese Academy of Sciences, Wenzhou, 325001, China

ARTICLE INFO

Keywords:
Aggregation-induced emission
Nano-sensors
Hypochlorite
Living cells and zebrafish

ABSTRACT

Hypochlorite (ClO^-) could be used as a diagnostic marker for inflammation and related diseases. Although there have been many reports on probes for ClO^- imaging, there was still a lack of specificity and anti-interference ability. Herein, carbazole (NEC) and tetraphenylethylene (TPE) equipped with thiobarbituric acid (TBA), **NEC-TBA** and **TPE-TBA**, were synthesized and used as a fluorescence biosensor for monitoring ClO^- with aggregation-induced emission (AIE) effect. we identified that **TPE-TBA**, with formed nanoparticles in the mean grain size at 76 nm (5 μM), was a superior probe to target ClO^- over other analytes with fluorescence "turn off" strategy. Subsequently, to explore the bioimaging application, **TPE-TBA** was able to sense exogenous ClO^- in living HeLa cells through fluorescence imaging. In zebrafish model, **TPE-TBA** effectively captured exogenous ClO^- in the entire organization of zebrafish. Overall, these AIE-based probes merit further development as organism targeting ClO^- sensors.

1. Introduction

Redox homeostasis of intra-cellular was of great importance in the field of physiology and pathology [1]. The destruction of redox homeostasis was closely related to some human diseases, such as cancer, neurological diseases, cardiovascular diseases, diabetes and gastrointestinal diseases [2–6]. Thus, cells have a fine regulatory system to maintain their redox balance, and can buffer changes in abnormal redox states by redox active molecules such as reactive oxygen, reactive nitrogen, activated carbon, and active sulfur [7–9]. These molecules undergo interaction and mutual transformation to promote a homeostasis of intracellular redox states. However, the most important oxidant in ROS was hypochlorous acid (HClO), which was a reactive oxygen molecule. The hypochlorous acid in the organism mainly produced by the catalytic action of peroxidase contains hydrogen peroxide (H_2O_2) and chloride ion (Cl^-) [10]. It plays an important role in the immune system, such as resistance to pathogenic microorganisms[11], resistance to viruses [12], and so on. When the concentration in the organism is unstable, it causes a series of diseases such as Parkinson's disease, Alzheimer's disease, cerebral ischemia and cancer [13–16]. Therefore, qualitative and quantitative detection of intracellular H_2S and HClO were of great significance. A series of detection methods have been developed in recent decades, such as colorimetry, electrochemical analysis, chromatographic analysis [17–19]. However, these methods are often cumbersome, and meanwhile, some work must be done in organic or organic/aqueous media to limit its application [20]. Compared with the above methods, the fluorescence detection method is widely used in biology because of its lower cost, higher selectivity and sensitivity, wider detection range, faster response time, and no damage to samples during the detection process [21,22]. At the same time, the detection process does little damage to the cells, and the combination of fluorescence detection and microscope can provide in vivo with real time response. Therefore, the detection of ClO^- by fluorescence has received widespread attention and significant development.

At present, many fluorescent probes for detecting hypochlorous acid have been reported, including BODIPY-based ClO^- fluorescent probe [23,24], rhodamine-based ClO^- fluorescent probe [25,26], fluorescein-based ClO^- fluorescent probe [27,28], and cyanine dye-based ClO^- Fluorescent probes [29,30], p-methoxyphenol-based ClO^- fluorescent probes [31,32], coumarin-based ClO^- fluorescent probes [33,34], and

* Corresponding author. Department of Urology, Nanfang Hospital, Southern Medical University, Guangzhou, 510515, China.
** Corresponding author.
E-mail addresses: shenjl@wibe.ac.cn (J. Shen), lulululu@smu.edu.cn (S. Zhao).
[1] These authors contributed equally to this work.

https://doi.org/10.1016/j.talanta.2020.120842
Received 11 November 2019; Received in revised form 13 February 2020; Accepted 13 February 2020
Available online 19 February 2020

metal complex-based ClO^- fluorescent probes [35–37]. These probes have their own advantages and disadvantages. Based on the above characteristics, a fluorescent probe based on aggregation induced luminescence (AIE) has been developed. This kind of organic small molecule fluorescent probe inherits the traditional organic molecular fluorescent probe. Advantages (such as high sensitivity, good selectivity, simple operation, real-time analysis, etc.) while overcoming its biggest drawbacks (aggregation-induced quenching, ACQ), which also gives good fluorescence at high concentrations or aggregates [32,38–40]. This makes it a significant advantage in the detection, imaging, etc. of various target ions or active small molecules in biological systems. Therefore, the synthesis of AIE-based organic small molecule fluorescent probes and their application in detection and imaging have become a research hotspot.

In this work, we have designed and synthesized two fluorescent probes carbazole-based (**NEC-TBA**) and tetraphenylethylene-based (**TPE-TBA**) to detect ClO^-. Tetraphenylethene derivatives, which have obviously AIE effect, and were used as the fluorophore, and carbazole was no AIE effect. Both of sensors were recognition ClO^- with "turn off" strategy, which the response mechanism of the probe toward ClO^- were confirmed with TEM and ^1H NMR. Furthermore, these two probes were successfully used for bioimaging ClO^- in living cells and zebrafish.

2. Experimental section

2.1. Materials and apparatus

Reagents were obtained from commercials and used as received without further purification. Sodium hypochlorite was purchased from Aladdin stored at 4 °C, and all of other chemicals were purchased from Aladdin and Sigma-Aldrich. HeLa cells were provided by ATCC (Manassas, VA) and zebrafish were got from the Animal Ethics Committee of Wenzhou Medical University. Absorption spectrum and emission spectrum were recorded on UV-2600 form SHIMADZU and RF-45301 from SHIMADZU, respectively. NMR spectra were obtained on a Bruker Ascend 400 spectrometer in DMSO-*d6*. Cells and zebrafish fluorescent images were acquired on confocal microscopy with Nikon-A1.

2.2. Synthesis and characterization of NEC-TBA

To a solution of 9-ethyl-9H-carbazole-3-carbaldehyde (250 mg, 1.12 mmol) in absolute ethanol (EtOH, 15 mL) was added 2-thioxodihydropyrimidine-4,6(1H,5H)-dione (241.9 mg, 1.68 mmol). After the reaction mixture was stirred at reflux for 4 h, the reaction mixture was filtered through a Buchner funnel, and filter cake was washed with ethanol to afford 312.7 mg of **NEC-TBA** as a red solid. Yield: 80%; ^1H NMR (600 MHz, DMSO-d_6) δ in ppm: 12.37 (s, 1H), 12.28 (s, 1H), 9.35 (d, J = 1.6 Hz, 1H), 8.68 (dd, J = 9.0, 1.6 Hz, 1H), 8.54 (s, 1H), 8.19 (d, J = 7.8 Hz, 1H), 7.75 (d, J = 9.0 Hz, 1H), 7.72 (d, J = 8.0 Hz, 1H), 7.62–7.49 (m, 1H), 7.34–7.31 (m, 1H), 4.52 (q, J = 7.2 Hz, 2H), 1.35 (t, J = 7.2 Hz, 3H); ^{13}C NMR (151 MHz, DMSO-d_6) δ in ppm: 178.78, 163.17, 160.82, 158.59, 143.71, 140.99, 134.40, 130.82, 127.52, 124.32, 123.15, 123.10, 121.32, 121.28, 114.75, 110.83, 109.90, 38.14, 14.43; HRMS (ESI) m/z $[M+1]^+$: Calcd for $C_{19}H_{16}N_3O_2S$, 350.0958, found, 350.0960.

2.3. Synthesis and characterization of TPE-TBA

To a solution of 4-(1,2,2-triphenylvinyl) benzaldehyde (250 mg, 8.2 mmol) in absolute ethanol (EtOH, 15 mL) was added 2-thioxodihydropyrimidine-4,6(1H,5H)-dione (177 mg, 1.23 mmol). After the reaction mixture was stirred at reflux for 4 h, the reaction mixture was filtered through a Buchner funnel, and filter cake was washed with ethanol to afford 297 mg of **TPE-TBA** as a yellow solid. Yield: 75%; ^1H NMR (600 MHz, DMSO-d_6) δ in ppm: 12.47 (s, 1H), 12.35 (s, 1H), 8.21 (s, 1H), 8.09 (d, J = 8.5 Hz, 2H), 7.33–7.15 (m, 9H), 7.12 (d, J = 8.5 Hz, 2H), 7.10–7.01 (m, 6H); ^{13}C NMR (151 MHz, DMSO-d_6) δ in ppm: 178.27, 161.63, 159.38, 154.76, 148.29, 142.62, 142.55, 142.39, 142.28, 139.63, 133.71, 130.58, 130.52, 130.49, 130.45, 130.39, 127.92, 127.88, 127.69, 126.94, 126.72, 118.24; HRMS (ESI) m/z $[M+1]^+$: Calcd for $C_{31}H_{23}N_2O_2S$, 487.1475, found, 487.1475.

2.4. Spectrum measurements

The stock solution of **NEC-TBA** and **TPE-TBA** were prepared in DMSO with the concentration of 10 mM, which prepared working solution with H_2O (0.1% DMSO) system in 20 μM and 10 μM for absorption spectrum and emission spectrum tests, respectively. The detecting ions (ClO^-) and other various interferential analytes stock solutions [GSH, Cys, NaHS, NaClO, Na_2SO_3, $NaHSO_3$ and H_2O_2] were prepared at 200 μM in deionized water. The work system solution contained **NEC-TBA** or **TPE-TBA**, H_2O (0.1% DMSO) and 5.0 equiv. of each analytes.

2.5. Cytotoxicity assays

The toxicological evaluation of **NEC-TBA** and **TPE-TBA** to HeLa cells were employed by traditional methods MTT assays [41]. HeLa cells were cultured and seeded in 96-well plates with 2×10^4 cells/mL, and after treatment by various concentrations of **NEC-TBA** and **TPE-TBA** from 0 μM to 100 μM at 37 °C for 24 h and 72 h. After that 10 μL MTT (5 mg/mL) was added to each well, and incubated with 4 h under the same condition, and was added 150 μL DMSO to dissolve precipitation after the supernatants were aspirated. To record the absorbance at 570 nm by microplate reader. The cell viability (%) = (ODs-ODb)/(ODc-ODb) × 100%, there s-sample, b-blank and c-control. All samples were repeated three times in parallel and averaged (n = 3).

2.6. Cell culture and imaging

Dulbecco's Modified Eagle Medium (DMEM, Hyclone) used for MRC-5 cells cultured, and 10% fetal calf serum (FBS, Sijiqing), penicillin (100 U/ml, Hyclone) and streptomycin sulfate (100 U/ml, Hyclone) were added in above medium, and cultured at 37 °C of 5% CO_2 and 95% air atmosphere condition [42]. HeLa cells were seeded in confocal dish processing for the night prior to imaging experiments. After that the cells were pretreated with 10 μM free **NEC-TBA** or **TPE-TBA** for 20 min, and then incubated with 50 μM of analytes including Cys, GSH, NaHS and NaClO for 20 min. Cellular imaging was performed after washing the cells thrice with PBS. Fluorescent imaging was taken in red channel on confocal microscopy with Nikon-A1.

2.7. Fluorescence imaging in zebrafish

The 5-day old zebrafish were cultured and transferred to 24-well plate, and 10 μM of free **NEC-TBA** or **TPE-TBA** was added for 20 min and washed with PBS, and then 50 μM of analytes including Cys, GSH, NaHS and NaClO were added respectively, which were incubated with 20 min further [43]. The zebrafish were washed and transferred to a new confocal dish for narcosis (3-Aminobenzoic acid ethyl ester methanesulfonate, MS222) and imaging.

3. Results and discussion

3.1. Design and synthesis of sensors

In this contribution, an AIE-based sensor could be used for detection with advantages of high tissue penetration, low cells damage and low fluorescence interference of biological tissues with better applications for biological detection and imaging. Based on this principle, the

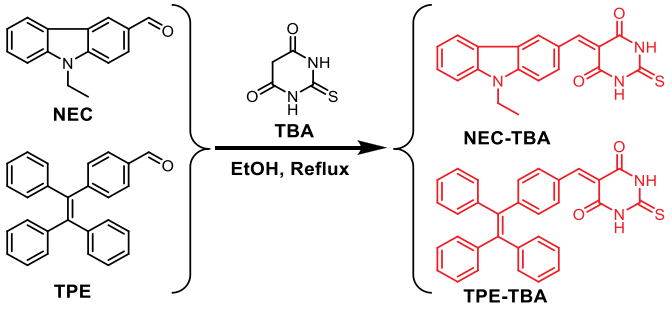

Scheme 1. Synthetic route of sensors **NEC-TBA** and **TPE-TBA**.

carbazole-based (**NEC-TBA**) (As a non-AIE structure, **NEC-TBA** was supplemented as a control) and tetraphenylethylene-based (**TPE-TBA**) biosensors were designed and synthesized from the reaction of thiobarbituric acid with carbazole-based aldehyde and tetraphenylethylene-based aldehyde, respectively (Scheme 1). The molecular structure was confirmed by NMR (^{1}H and ^{13}C) and mass spectrum as shown in Figs. S1–S3. The absorption spectra of **NEC-TBA** and **TPE-TBA** in DMSO and H_2O solution system were presented in Fig. 1. Both of them have optimum excitation wavelength peaks (Ex) at 488 nm and 435 nm in DMSO solution system, which were contributed to the electron π–π* transition on moiety. Meanwhile, both of them have optimum excitation wavelength peaks (Ex) at 480 nm and 455 nm in H_2O solution system with a blue shift compared to DMSO system.

3.2. Proposed sensing mechanism

To confirm the sensing mechanism of **NEC-TBA** and **TPE-TBA** for detecting ClO^-, the reaction product of **TPE-TBA** with ClO^- was were characterized by ^{1}H NMR and MS. The probe **TPE-TBA** structure has a very good conjugated system and exhibits strong red fluorescence. With addition of sodium hypochlorite, the original conjugated system of the probe was destroyed due to the oxidation of hypochlorite, which was caused probe fluorescence to quench. In order to verify the above conjecture, mass spectrometry was performed on the probe **TPE-TBA**

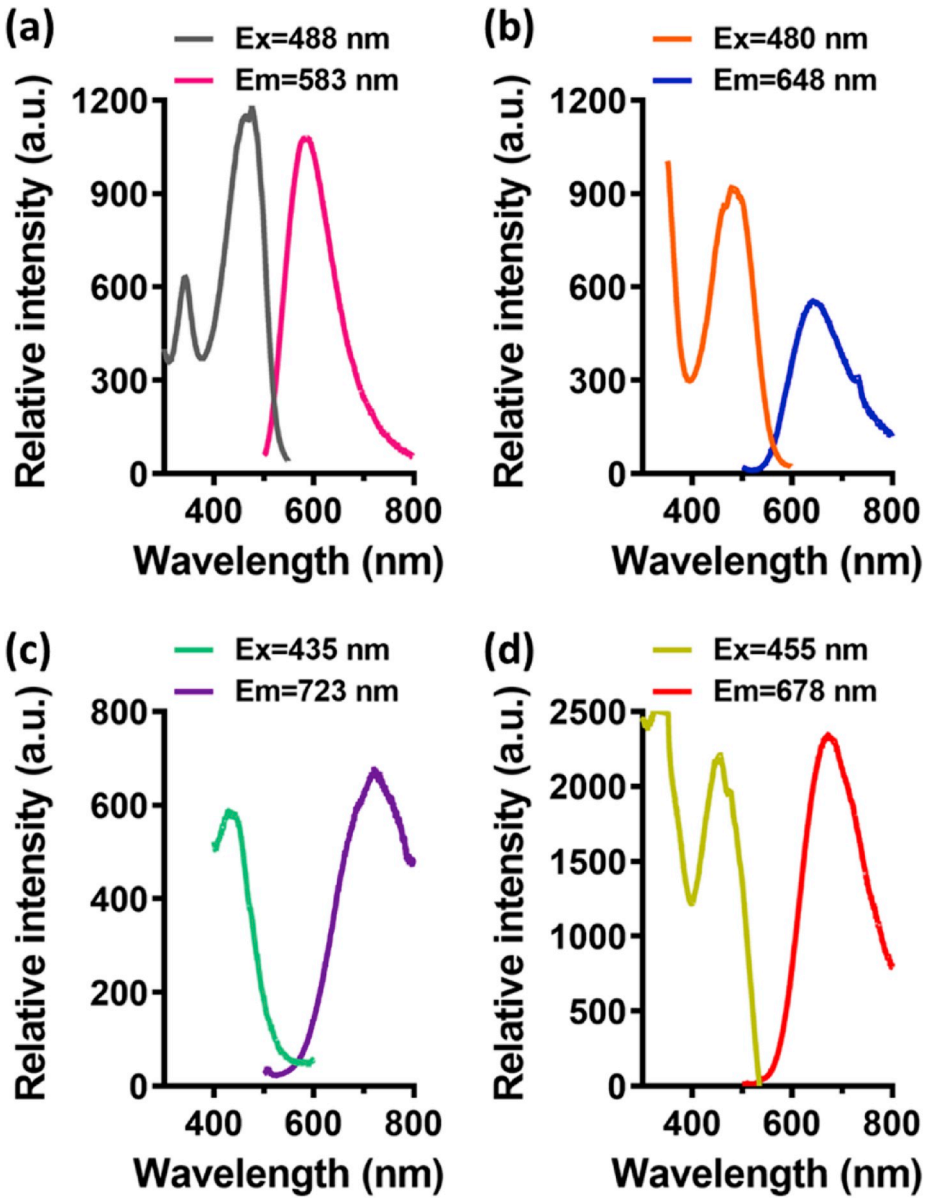

Fig. 1. The normalized absorption and fluorescence spectra of sensors **NEC-TBA** in DMSO (a) and H_2O (b), and **TPE-TBA** in DMSO (c) and H_2O (d) solution system.

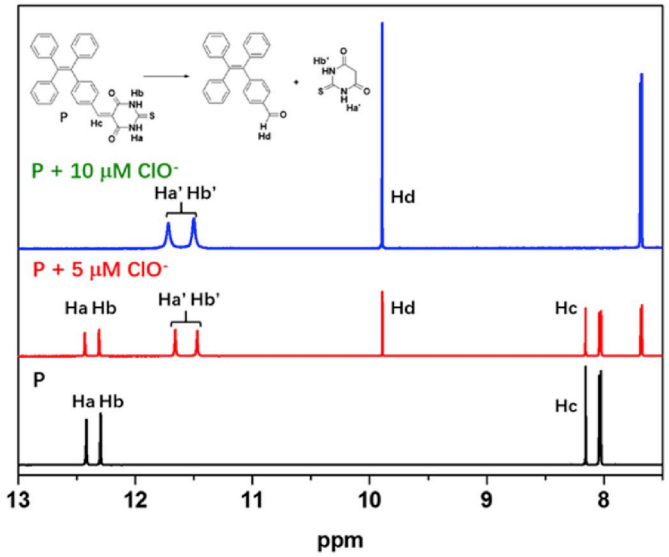

Fig. 2. ^{1}H NMR spectra titration of **TPE-TBA** after treatment with different concentrations of NaClO in D_2O (400 MHz).

solution to which sodium hypochlorite solution was added. Mass spectrometry showed that the signal peak of m/z = 361.15 and 145.00 appeared in the reaction solution, which were tetrastyrene aldehyde (m/z = 360.15) and thiobarbituric acid (m/z = 144.00) fragments respectively, and the mass spectrum signal peak of the probe **TPE-TBA** was [M + H] = 487.15 (Fig. S3). This indicates that the probe **TPE-TBA** was oxidized in the action of hypochlorous acid with the C═C bond was broken, and the original product were formed. The above results indicate that the probe **TPE-TBA** was oxidized under the action of hypochlorous acid to form tetrastyrene aldehyde and thiobarbituric acid, and the original conjugated system was destroyed, thereby generating a change in the fluorescent signal. To gain some insights of the binding mode of **TPE-TBA** with ClO^-, we studied the oxidation products by ^{1}H NMR spectrum titration (Fig. 2).When 0, 5, 10 μM ClO^- was separately added to **TPE-TBA**, one of the two –NH signal at 12.47 and 12.35 was shifted to 11.54 and 11.5 ppm and the other at 9.96 ppm appeared gradually, the *HC*═C signal at δ 8.21 and 8.09 ppm disappeared completely with the same time, which support the notion that the C═C group of **TPE-TBA** between the tetrastyrene aldehyde and thiobarbituric acid was fractured with oxidation of ClO^-. Moreover, we studied the nanoaggregates using transmission electron microscope (TEM) and dynamic light scattering (DLS). The formation of spherical nanoaggregates with a diameter in the range 60–90 nm has been observed by TEM as shown in Fig. 3, this size was smaller than that (~100 nm) determined by the DLS (Fig. S4). As previously reported[44,45], **TPE-TBA** has an AIE structure, which can aggregate to form nanoparticles in aqueous systems, whereas the **NEC-TBA** structure does not have the AIE effect, and it is in the form of a solution .

3.3. Absorption and emission spectrum titration

The absorption titration of fluorescence probe was initially investigated with various amounts of ClO^-. As shown in Fig. S5, the **NEC-TBA** in H_2O solution displayed two absorption bands at 338 nm and 480 nm respectively, which might be ascribed to the corresponding thiobarbituric acid moiety and carbazole moiety. The absorbance of signals at 338 nm and 480 nm decreased step by step with the increase of ClO^- respectively, presenting that the conjugated system of the molecule structure was changed due to reaction between **NEC-TBA** and ClO^-. The absorption profile was changed when 5.0 equivalents of ClO^- was introduced. **TPE-TBA** exhibits evident bands around 435 nm. Upon addition of ClO^- (5.0 equivalent), the absorption intensity of signals was faded, which further confirms the reaction between **TPE-TBA** and ClO^-. The fluorescence spectra of **NEC-TBA** in the presence of various concentrations of ClO^- in H_2O solution were shown to Fig. 4. With excited at 480 nm, free **NEC-TBA** presented strong fluorescence peaked at 648 nm. With increase concentrations of ClO^- led to a prominent fluorescence faded away, and fluorescence quenched with 5.0 equivalents of ClO^- added. Moreover, upon excitated at 455 nm, the free **TPE-TBA** exhibited obvious emission spectra at 678 nm. The fluorescent intensity at 678 nm decreased step by step with addition of ClO^-, and the fluorescence quenched and remained stable upon the addition of 5.0 equivalents of ClO^- (Fig. 4).

In order to study the selectivity of **NEC-TBA** and **TPE-TBA**, we selected a lot of analytes for fluorescence titration detection. It can be seen from Fig. S6 that when other analytes were added to **NEC-TBA**, and the fluorescent signal of **NEC-TBA** were decreased and disappeared shown in Fig. S6. However, gradually adding the corresponding analytes to **TPE-TBA** did not produce a significant change in the fluorescence of **TPE-TBA** shown in Fig. S7. The results show that **TPE-TBA** has good selectivity compared to **TPE-TBA**. The limit of detection (LOD) of sensors for ClO- were calculated based on 3δ/K, δ was the standard deviation of the blank sample and K was the slope of the linear regression equation. As shown in Fig. S8, the LOD of **NEC-TBA** and **TPE-TBA** were calculated for 312 nM and 334 nM, respectively, which was comparable to previously reported ClO^- proportional fluorescent probes (Table S1). These results indicate that both of sensors could be detected ClO^- with high sensitivity.

3.4. Cells imaging

With excellent properties, the potential biological application of **NEC-TBA** and **TPE-TBA** for fluorescent imaging of ClO^- in living HeLa cells was studied. Cell bioimaging were executed in HeLa cell lines. The

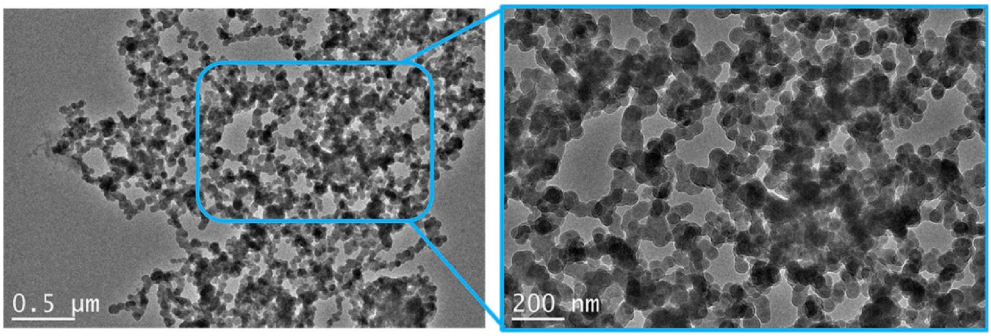

Fig. 3. Transmission electron microscope images of the **TPE-TBA** (10 μM), and local amplification analysis.

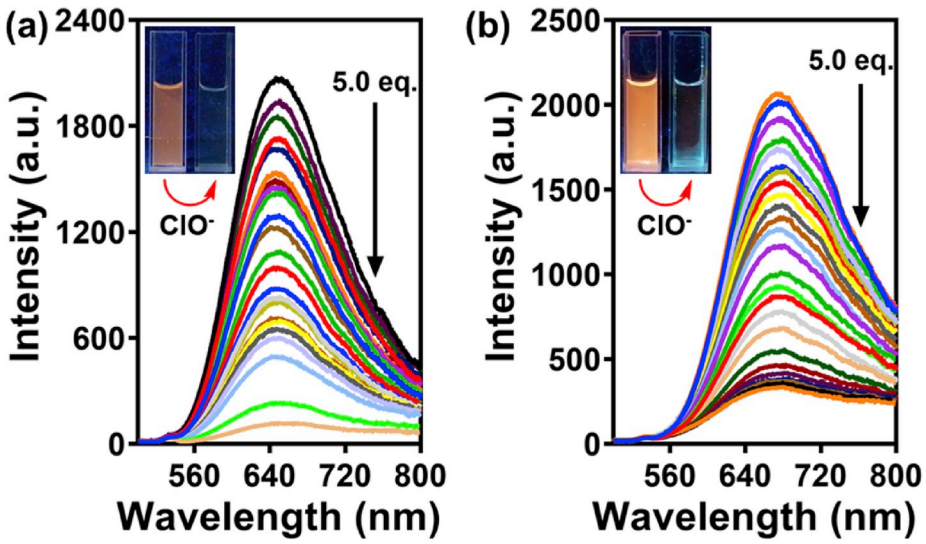

Fig. 4. Fluorescence spectra (10 μM) of **NEC-TBA** (a) and **TPE-TBA** (b) as well as the color change (insets) with addition of ClO^- (5.0 eq.) at in water solution system. (For interpretation of the references to color in this figure legend, the reader is referred to the Web version of this article.)

cytotoxicity of **NEC-TBA** and **TPE-TBA** were evaluated by traditional MTT assay, and the results exhibited that about 70% of cells still remained alive even though 20 μM probes were normalized for 24 h and 72 h (Fig. S9), revealing **NEC-TBA** and **TPE-TBA** had low cytotoxicity and could be further used for cell imaging experiments. Subsequently, to demonstrate the capability of probe to sense exogenous ClO^- in cells, we performed imaging assay with negative and positive control as powerful evidence. Cell lines were stained with probes (10 μM) at 37 °C for 20 min after washed thrice with PBS. Under the above system, ClO^- (50 μM) were added and incubated for 20 min at 37 °C further, respectively. As shown in Fig. 5, when incubated only **NEC-TBA** in HeLa cells, the luminous red fluorescence of **NEC-TBA** was found in the cytoplasm. Whereas, when the cell culture was incubated with a concentration of NaClO, GSH, Cys and NaHS (50 μM) respectively, and the

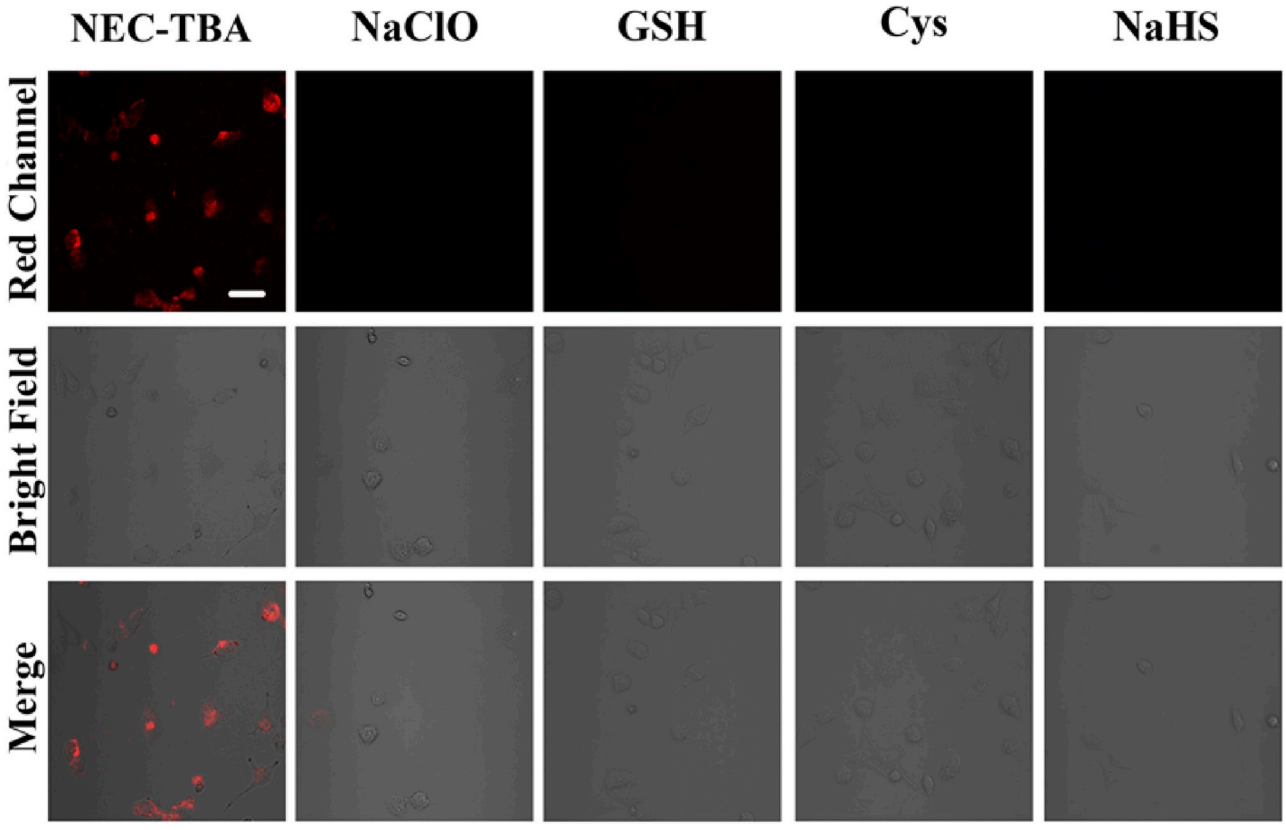

Fig. 5. Confocal fluorescence images of HeLa cells. HeLa cells were incubated with **NEC-TBA** (10 μM) for 20 min, further incubated with 50 μM NaClO, GSH, Cys and NaHS for 20 min, respectively.

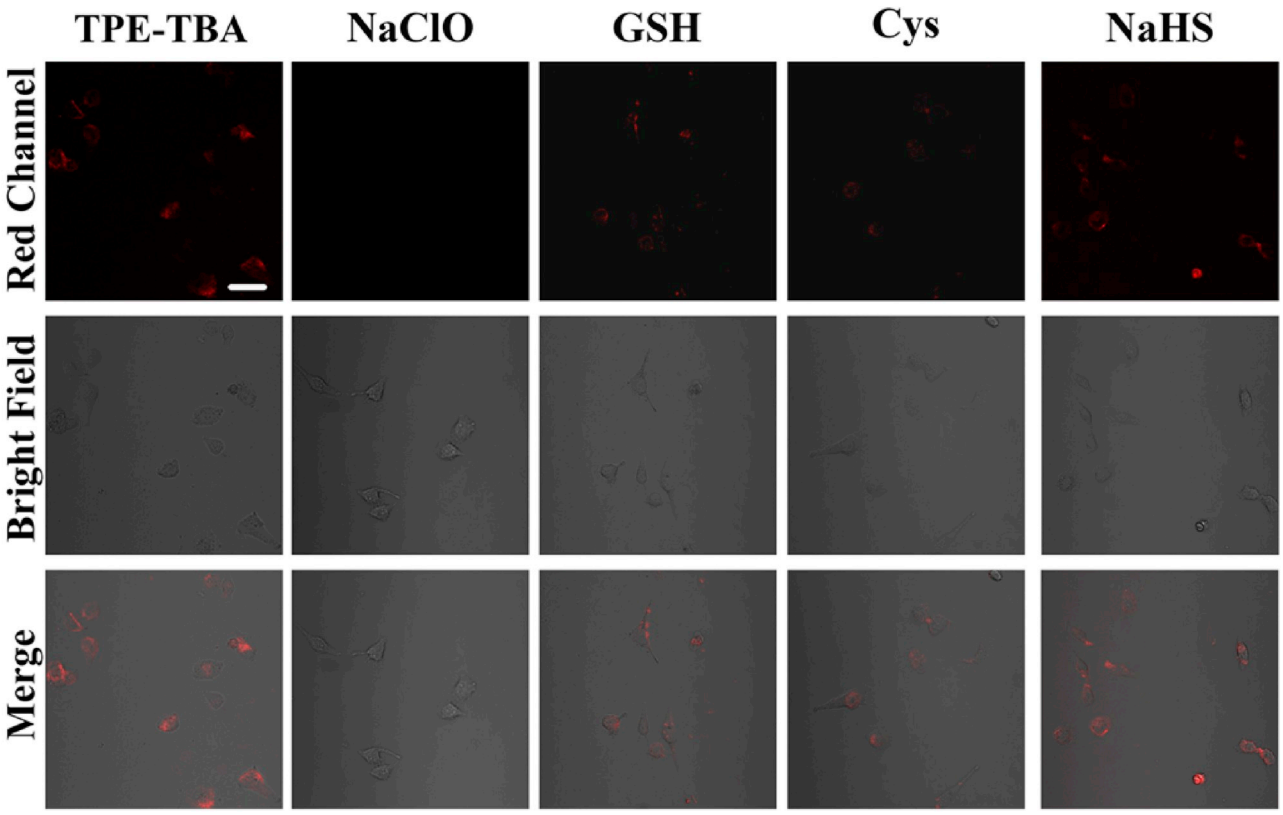

Fig. 6. Confocal fluorescence images of HeLa cells. HeLa cells were incubated with **TPE-TBA** (10 μM) for 20 min, further incubated with 50 μM NaClO, GSH, Cys and NaHS for 20 min, respectively.

cells start to show no fluorescence in the cytoplasm. However, the remarkable fluorescence was found in the red channel when the cells were pretreated with **TPE-TBA**, which was illustrated that this probe has a good cell permeability as shown in Fig. 6. While, a disappeared of fluorescence signal was observed with incubated with ClO^- furtherly. In comparison, the insusceptible fluorescence intensity in the red channel were observed with addition of 50 μM other analytes including GSH, Cys and NaHS, which was suggested that **TPE-TBA** could be capable of sensing ClO^- for specificity. Thus, these results clearly indicated that the **TPE-TBA** probe meet the requirements for monitoring of exogenous ClO^- in living cells.

3.5. Zebrafish imaging

With normal metabolic processes, organisms can spontaneously produce various ROS (ClO^-) through organs, and the body also regulates the redox homeostasis through ClO^- in organism. Therefore, monitoring the content of ClO^- in organisms by fluorescent probe method has potential research value. Most of studies reported have demonstrated that the possibility of fluorescence imaging was restricted to cell level. However, biological imaging of ClO^- by fluorescent probes in normal organisms still faces the problem of sensitivity and stability of the probe and its ability to pass various biological barriers. To get insight into the feasibility of **NEC-TBA** and **TPE-TBA** respond to ClO^-, five-days-old zebrafish, a popular vertebrate model, were chosen as our research model system. As Fig. 7 shown that the zebrafish were cultured in embryo medium, and incubated with **NEC-TBA** (10 μM) for 20 min to insured sensor to permeate into the whole tissues of zebrafish, which exhibited a visible red fluorescence in zebrafish, which were showed that **NEC-TBA** could response to exogenous ClO^- in zebrafish with good biocompatibility. There was almost no fluorescence was found in the red channel when the zebrafish were pretreated with ClO^- (50 μM), which fluorescence quenching by exogenous ClO^-. In addition, the zebrafish pretreated with **NEC-TBA** and washed thrice with PBS, and further incubated with 50 μM GSH, Cys and NaHS respectively, which were displayed the similar results as ClO^- with fluorescence quenching. Subsequently, probe TPE-TBA was addition in zebrafish as shown in Fig. 8, which exhibited a prominent red fluorescence in whole of zebrafish. However, the zebrafish pretreated with TPE-TBA, and further incubated with NaClO, GSH, Cys and NaHS (50 μM) respectively, which displayed only ClO- group was on fluorescence signal, while GSH, Cys and NaHS group had no effect on TPE-TBA imaging in zebrafish with the same results to cells imaging experiment, which were might be due to the formation of nanoparticles by TPE-TBA, and consistent with the results described in the previous spectroscopy data. Collectively, all these results convincingly indicated that TPE-TBA possessed the high tissue penetration capacity and could be realized the visualization of ClO^- in organism, which have a potential application for living imaging to response ClO^-. The above results indicate that TPE-TBA has potential application for bioimaging in living biosystem.

4. Conclusions

In summary, there was designed and synthesized a carbazole-based and tetraphenylethylene-based fluorescent probe **NEC-TBA** and **TPE-TBA** employing TBA group as the recognition receptor of ClO^-. **TPE-TBA** exhibits excellent selectivity toward ClO^- over other analytes, including Cys, GSH, SO_3^{2-}, HS^- and HSO_3^-, which might be contributed to the oxidative cleavage of **TPE-TBA** moiety via the isolation of TBA group to form aldehyde group. Meanwhile, **TPE-TBA** could be formed nanoparticles to avoid the oxidization by other analytes except for ClO^-. Moreover, experiments on bioimaging applications demonstrate **TPE-TBA** can specifically monitor the exogenous of cellular ClO^- levels from HeLa cells with low cytotoxicity. Subsequently, to take advantages of penetrability imaging in zebrafish, the results shown that

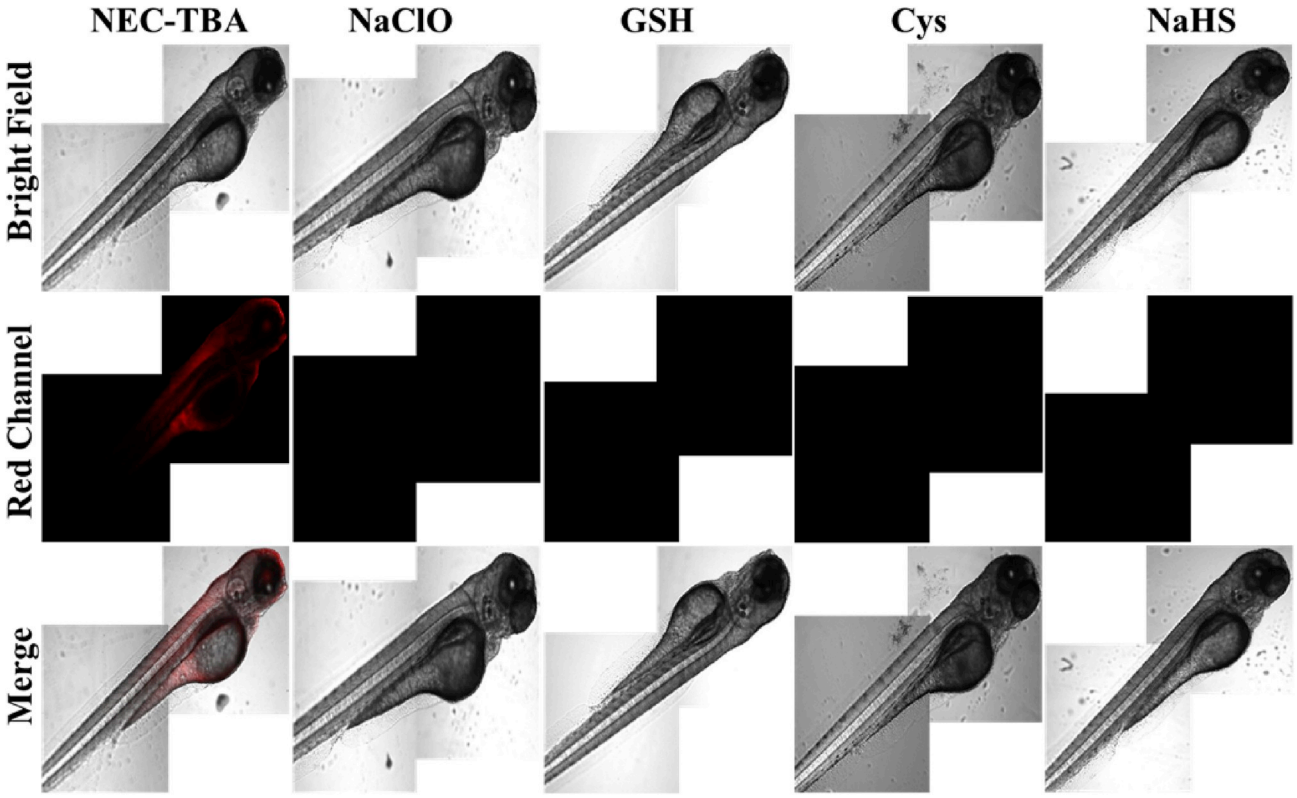

Fig. 7. Confocal fluorescence images of zebrafish. 5-days-old zebrafish were incubated with **NEC-TBA** (10 μM) for 20 min and washed with PBS, further incubated with 50 μM NaClO, GSH, Cys and NaHS for 20 min, respectively.

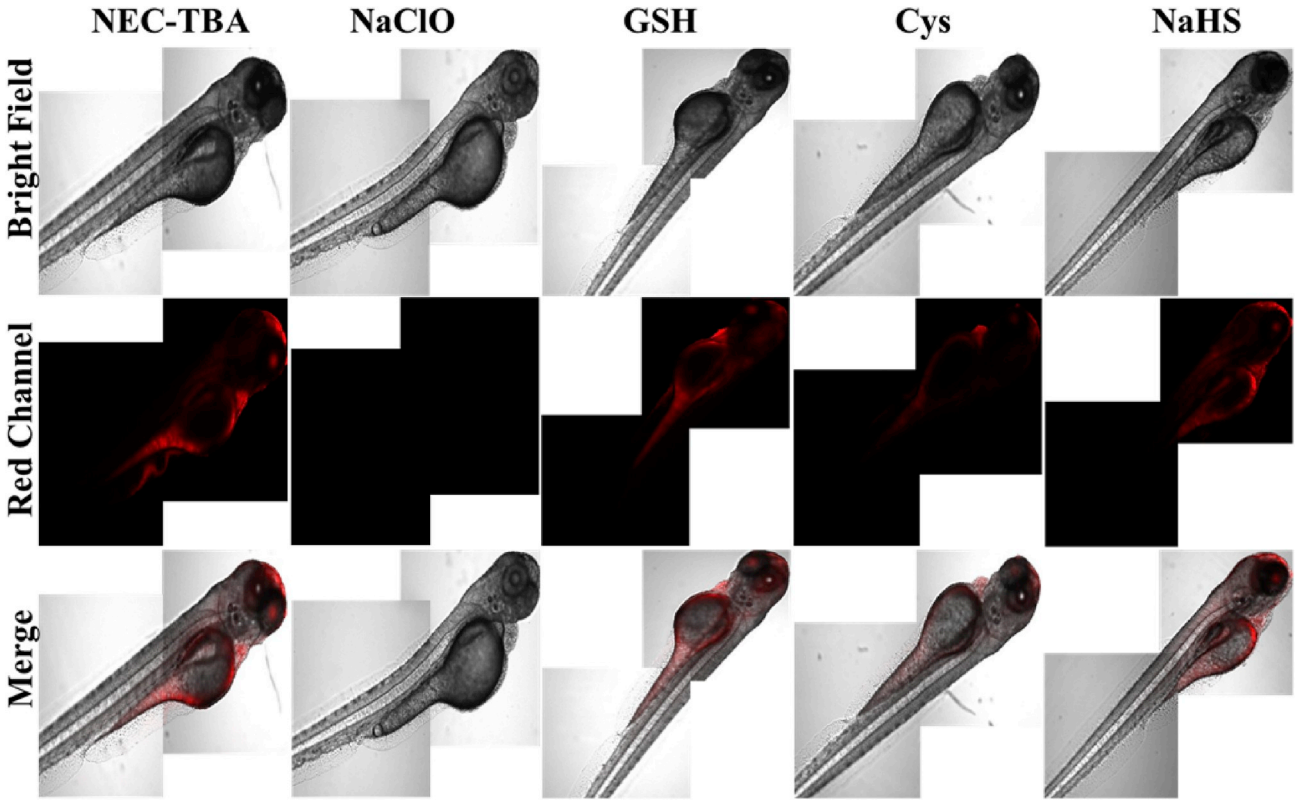

Fig. 8. Confocal fluorescence images of zebrafish. 5-days-old zebrafish were incubated with **TPE-TBA** (10 μM) for 20 min and washed with PBS, further incubated with 50 μM NaClO, GSH, Cys and NaHS for 20 min, respectively.

TPE-TBA has been successfully monitored and imaged exogenous of ClO^- in zebrafish.

CRediT authorship contribution statement

Hong Chen: Conceptualization, Methodology, Software, Data curation, Writing - original draft. **Xiaojun He:** Conceptualization, Methodology, Software, Data curation, Writing - original draft. **Yuzhong Yu:** Visualization, Investigation. **Yuna Qian:** Software, Validation. **Jianliang Shen:** Writing - review & editing. **Shanchao Zhao:** Supervision, Funding acquisition, Project administration, Writing - review & editing.

Declaration of competing interest

Author has no conflicts of interest with the published study.

Acknowledgements

This work was financially supported by the National Natural Science Foundation of China (Nos. 81972394 and 31800833), the Science and Technology Planning Projects of Guangdong Province (No. 2016A020215175), the Natural Science Foundation of Guangdong Province (No. 2016A030313583), the Medical Scientifc Research Foundation of Guangdong Province (No. A2016555), the Outstanding Youths Development Scheme of Nanfang Hospital, Southern Medical University (No. 2015J005) and the Science and Technology Planning Project of Guangzhou (No. 201704020070).

Appendix A. Supplementary data

Supplementary data to this article can be found online at https://doi.org/10.1016/j.talanta.2020.120842.

References

[1] A.A. Alfadda, R.M. Sallam, Reactive oxygen species in health and disease, BioMed Res. Int. 2012 (2012).
[2] M. Smith, R. Hunter, N. Stellenboom, D.A. Kusza, M.I. Parker, A.N. Hammouda, et al., The cytotoxicity of garlic-related disulphides and thiosulfonates in WHCO1 oesophageal cancer cells is dependent on S-thiolation and not production of ROS, Biochim. Biophys. Acta Gen. Subj. 1860 (7) (2016) 1439–1449.
[3] L. Liu, K. Zhang, H. Sandoval, S. Yamamoto, M. Jaiswal, E. Sanz, et al., Glial lipid droplets and ROS induced by mitochondrial defects promote neurodegeneration, Cell 160 (1–2) (2015) 177–190.
[4] T. Vanessa Fiorentino, A. Prioletta, P. Zuo, F. Folli, Hyperglycemia-induced oxidative stress and its role in diabetes mellitus related cardiovascular diseases, Curr. Pharmaceut. Des. 19 (32) (2013) 5695–5703.
[5] J. Lund, D.M. Ouwens, M. Wettergreen, S.S. Bakke, G.H. Thoresen, V. Aas, Increased glycolysis and higher lactate production in hyperglycemic myotubes, Cells 8 (9) (2019) 1101.
[6] A. Bhattacharyya, R. Chattopadhyay, S. Mitra, S.E. Crowe, Oxidative stress: an essential factor in the pathogenesis of gastrointestinal mucosal diseases, Physiol. Rev. 94 (2) (2014) 329–354.
[7] M. Hardy, J. Zielonka, H. Karoui, A. Sikora, R. Michalski, R. Podsiadły, et al., Detection and characterization of reactive oxygen and nitrogen species in biological systems by monitoring species-specific products, Antioxidants Redox Signal. 28 (15) (2018) 1416–1432.
[8] J. Park, Y. Joe, S.W. Ryter, Y.-J. Surh, H.T. Chung, Similarities and distinctions in the effects of metformin and carbon monoxide in immunometabolism, Mol. Cell. 42 (4) (2019) 292.
[9] B. Ezraty, A. Gennaris, F. Barras, J.-F. Collet, Oxidative stress, protein damage and repair in bacteria, Nat. Rev. Microbiol. 15 (7) (2017) 385.
[10] I. Kowanko, E. Bates, A. Ferrante, Mechanisms of human neutrophil-mediated cartilage damage in vitro: the role of lysosomal enzymes, hydrogen peroxide and hypochlorous acid, Immunol. Cell Biol. 67 (5) (1989) 321–329.
[11] C. Staerck, A. Gastebois, P. Vandeputte, A. Calenda, G. Larcher, L. Gillmann, et al., Microbial antioxidant defense enzymes, Microb. Pathog. 110 (2017) 56–65.
[12] J. Wu, R. Yang, Z. Yang, S. Yao, S. Zhao, Y. Wang, et al., ROS accumulation and antiviral defence control by microRNA528 in rice, Nature plants 3 (1) (2017) 16203.
[13] A. Lan, J. Chen, Z. Chai, Y. Hu, The neurotoxicity of iron, copper and cobalt in Parkinson's disease through ROS-mediated mechanisms, Biometals : an international journal on the role of metal ions in biology, biochemistry, and medicine 29 (4) (2016) 665–678.
[14] W.T. Wang, B.A. Tailor, D.S. Cohen, X. Huang, Alzheimer's pathogenesis, metal-mediated redox stress, and potential nanotheranostics, EC pharmacology and toxicology 7 (7) (2019) 547.
[15] C. Zhang, C-l Ling, L. Pang, Q. Wang, J-x Liu, B-s Wang, et al., Direct macromolecular drug delivery to cerebral ischemia area using neutrophil-mediated nanoparticles, Theranostics 7 (13) (2017) 3260.
[16] Y. Feng, S. Liao, C. Wei, D. Jia, K. Wood, Q. Liu, et al., Infiltration and persistence of lymphocytes during late-stage cerebral ischemia in middle cerebral artery occlusion and photothrombotic stroke models, J. Neuroinflammation 14 (1) (2017) 248.
[17] X. Chen, F. Wang, J.Y. Hyun, T. Wei, J. Qiang, X. Ren, et al., Recent progress in the development of fluorescent, luminescent and colorimetric probes for detection of reactive oxygen and nitrogen species, Chem. Soc. Rev. 45 (10) (2016) 2976–3016.
[18] Y. Li, K. Hu, Y. Yu, S.A. Rotenberg, C. Amatore, M.V. Mirkin, Direct electrochemical measurements of reactive oxygen and nitrogen species in nontransformed and metastatic human breast cells, J. Am. Chem. Soc. 139 (37) (2017) 13055–13062.
[19] Q. Wang, M.-H. Zou, Measurement of Reactive Oxygen Species (ROS) and Mitochondrial ROS in AMPK Knockout Mice Blood Vessels, Springer, AMPK, 2018, pp. 507–517.
[20] Z. Zhou, H. Wu, F. Li, L. Ma, X. Qiao, Hypochlorite responsive ratiometric fluorescent switch and logic gates based on lanthanide functionalized polymer nanosphere, Dyes Pigments 174 (2020) 108033.
[21] Y. Dai, C.C. Liu, Recent advances on electrochemical biosensing strategies toward universal point-of-care systems, Angew. Chem. Int. Ed. 58 (36) (2019) 12355–12368.
[22] Z. Zhou, J. Gu, X. Qiao, H. Wu, H. Fu, L. Wang, et al., Double protected lanthanide fluorescence core@ shell colloidal hybrid for the selective and sensitive detection of ClO−, Sensor. Actuator. B Chem. 282 (2019) 437–442.
[23] H. Zhu, J. Fan, J. Wang, H. Mu, X. Peng, An "enhanced PET"-based fluorescent probe with ultrasensitivity for imaging basal and elesclomol-induced HClO in cancer cells, J. Am. Chem. Soc. 136 (37) (2014) 12820–12823.
[24] G. Cheng, J. Fan, W. Sun, K. Sui, X. Jin, J. Wang, et al., A highly specific BODIPY-based probe localized in mitochondria for HClO imaging, Analyst 138 (20) (2013) 6091–6096.
[25] Q.-P. Zuo, Z.-J. Li, Y.-H. Hu, B. Li, L.-H. Huang, C.-J. Wang, et al., A highly sensitive fluorescent probe for HClO and its application in live cell imaging, J. Fluoresc. 22 (5) (2012) 1201–1207.
[26] H. Zhang, J. Liu, C. Liu, P. Yu, M. Sun, X. Yan, et al., Imaging lysosomal highly reactive oxygen species and lighting up cancer cells and tumors enabled by a Si-rhodamine-based near-infrared fluorescent probe, Biomaterials 133 (2017) 60–69.
[27] Z. Zhan, R. Liu, L. Chai, Q. Li, K. Zhang, Y. Lv, Turn-on fluorescent probe for exogenous and endogenous imaging of hypochlorous acid in living cells and quantitative application in flow cytometry, Anal. Chem. 89 (17) (2017) 9544–9551.
[28] R. Zhang, J. Zhao, G. Han, Z. Liu, C. Liu, C. Zhang, et al., Real-time discrimination and versatile profiling of spontaneous reactive oxygen species in living organisms with a single fluorescent probe, J. Am. Chem. Soc. 138 (11) (2016) 3769–3778.
[29] G. Cheng, J. Fan, W. Sun, J. Cao, C. Hu, X. Peng, A near-infrared fluorescent probe for selective detection of HClO based on Se-sensitized aggregation of heptamethine cyanine dye, Chem. Commun. 50 (8) (2014) 1018–1020.
[30] X. Zhang, W. Zhao, B. Li, W. Li, C. Zhang, X. Hou, et al., Ratiometric fluorescent probes for capturing endogenous hypochlorous acid in the lungs of mice, Chem. Sci. 9 (43) (2018) 8207–8212.
[31] Y. He, Y. Xu, Y. Shang, S. Zheng, W. Chen, Y. Pang, An ESIPT-based fluorescent probe for the determination of hypochlorous acid (HClO): mechanism study and its application in cell imaging, Anal. Bioanal. Chem. 410 (27) (2018) 7007–7017.
[32] R. Shi, H. Chen, Y. Qi, W. Huang, G. Yin, R. Wang, From aggregation-induced to solution emission: a new strategy for designing ratiometric fluorescent probes and its application for in vivo HClO detection, Analyst 144 (5) (2019) 1696–1703.
[33] J. Fan, H. Mu, H. Zhu, J. Wang, X. Peng, Light up ClO(-) in live cells using an aza-coumarin based fluorescent probe with fast response and high sensitivity, Analyst 140 (13) (2015) 4594–4598.
[34] W.L. Wu, H.L. Ma, L.L. Xi, M.F. Huang, K.M. Wang, J.Y. Miao, et al., A novel lipid droplets-targeting ratiometric fluorescence probe for hypochlorous acid in living cells, Talanta 194 (2019) 308–313.
[35] Q.Y. Li, Y.A. Li, Q. Guan, W.Y. Li, X.J. Dong, Y.B. Dong, UiO-68-PT MOF-based sensor and its mixed matrix membrane for detection of HClO in water, Inorg. Chem. 58 (15) (2019) 9890–9896.
[36] Y.A. Li, S. Yang, Q.Y. Li, J.P. Ma, S. Zhang, Y.B. Dong, UiO-68-ol NMOF-based fluorescent sensor for selective detection of HClO and its application in bioimaging, Inorg. Chem. 56 (21) (2017) 13241–13248.
[37] H. Li, C. Wang, T. Hou, F. Li, Amphiphile-mediated ultrasmall aggregation induced emission dots for ultrasensitive fluorescence biosensing, Anal. Chem. 89 (17) (2017) 9100–9107.
[38] D. Ding, K. Li, B. Liu, B.Z. Tang, Bioprobes based on AIE fluorogens, Accounts Chem. Res. 46 (11) (2013) 2441–2453.
[39] J. Chang, X. Wang, J. Wang, H. Li, F. Li, Nucleic acid-functionalized metal–organic framework-based homogeneous electrochemical biosensor for simultaneous detection of multiple tumor biomarkers, Anal. Chem. 91 (5) (2019) 3604–3610.
[40] X. Li, J. Gu, Z. Zhou, W. Liu, J. Gao, Q. Wang, Precise control for the aggregation and deaggregation with the aid of a tetraphenylethylene derivative: luminescence modulation and sensing performance, Dyes Pigments 172 (2020) 107844.
[41] H.L. Ciliao, D.L. Ribeiro, R.B. Camargo-Godoy, A.F. Specian, J.M. Serpeloni, I.M. Colus, Cytotoxic and genotoxic effects of high concentrations of the immunosuppressive drugs cyclosporine and tacrolimus in MRC-5 cells, Exp. Toxicol. Pathol. : official journal of the Gesellschaft fur Toxikologische Pathologie 67 (2) (2015) 179–187.
[42] J. Chen, G. Wang, L. Li, P. Zhang, Protective effect of Astragalus polysaccharide on

MRC-5 cells from oxidative damage induced by hydrogen peroxide, Xi bao yu fen zi mian yi xue za zhi = Chinese journal of cellular and molecular immunology 31 (8) (2015) 1062–1066.
[43] X. He, C. Wu, Y. Qian, Y. Li, F. Ding, Z. Zhou, et al., Symmetrical bis-salophen probe serves as a selectively and sensitively fluorescent switch of gallium ions in living cells and zebrafish, Talanta 205 (2019) 120118.
[44] W. Bai, Z. Wang, J. Tong, J. Mei, A. Qin, J.Z. Sun, et al., A self-assembly induced emission system constructed by the host–guest interaction of AIE-active building blocks, Chem. Commun. 51 (6) (2015) 1089–1091.
[45] H. Xie, F. Zeng, S. Wu, Ratiometric fluorescent biosensor for hyaluronidase with hyaluronan as both nanoparticle scaffold and substrate for enzymatic reaction, Biomacromolecules 15 (9) (2014) 3383–3389.